Fermi National Accelerator Laboratory

FERMILAB-Conf-95/001-E

CDF

CDF Calorimeter and Its Upgrade

Y. Seiya
The CDF Collaboration

Fermi National Accelerator Laboratory
P.O. Box 500, Batavia, Illinois 60510

Institute of Physics, University of Tsukuba
Tsukuba-Shi, Ibaraki-ken 305, Japan

January 1995

Proceedings of the *1994 Beijing Calorimetry Symposium at IHEP*, Beijing, October 25-27, 1994.

Operated by Universities Research Association Inc. under Contract No. DE-AC02-76CHO3000 with the United States Department of Energy

Disclaimer

CDF/PUB/CALORIMETRY/PUBLIC/2911
FERMILAB-CONF-95/001-E

CDF Calorimeter and its Upgrade[1]

Y. Seiya
Institute of Physics, University of Tsukuba,
Tsukuba-shi, Ibaraki-ken 305, Japan

For the CDF collaboration

[1] For the proceedings of 1994 Beijing Calorimetry Symposium on 25–27 Oct at IHEP, Beijing

CDF Calorimeter and its Upgrade

Y. Seiya

Institute of Physics, University of Tsukuba,
Tsukuba-shi, Ibaraki-ken 305, Japan

The CDF calorimeter systems are briefly reviewed with an emphasis on the calibration and the performance of the central electromagnetic calorimeter. Several physics analyses where the calorimetry plays an important role are discussed. The present gas calorimeter will be upgraded in accord with the collider upgrade. The new system is a scintillator-based calorimeter with optical fiber readout. A status of the CDF calorimeter upgrade project is also described.

1. Introduction

A colliding experiment has been conducted at Fermilab since 1987 using Tevatron. The Tevatron is the first collider with full use of superconducting magnets and provides proton-antiproton collisions at the center of mass energy of 1.8 TeV. The CDF (Collider Detector at Fermilab) detector is located at one of two interaction points along the Tevatron ring.

The first collision was observed in October of 1985. In 1987, the test physics run was carried out and recorded data of 25 nb^{-1}. The first physics run followed it from 1988 to 1989 collecting 4 pb^{-1} of data. After a test beam term from 1990 to 1992, the physics run called run IA started in April of 1992 and completed in May of 1993 resulting in a 19 pb^{-1} of data. Run IB started in December of 1993 and is still running as of December 1994.

2. Design of the CDF Calorimeter

The CDF is a general purpose detector built to explore $p\bar{p}$ collisions at $\sqrt{s} = 1.8$ TeV. It consists of 3 major parts, central, forward and backward detectors, and covers almost full solid angle. The detector is forward-backward symmetric. The central part is further divided to the central and plug detectors. There is a 1.5 T magnetic field generated by a superconducting solenoid in order to measure particles' momenta. Exploiting implemented detector subsystems, the CDF detector is capable of identifying electrons, photons, muons, neutrinos as a presence of missing transverse energy , and jets.

It is useful to list the detector components in the central region seen by particles emitting from the interaction point in order to give an idea of the detector structure. After passing the beam pipe, particles serially go through the silicon vertex detector, the vertex time projection chamber, central tracking chamber, central drift tube, (solenoid), central pre-radiator, central electromagnetic calorimeter, central hadron calorimeter, central muon chamber, (50 cm steel), and another central muon chamber system.

The CDF calorimeter has a projective tower geometry with a fine granularity. There are 7 calorimeter systems, central electromagnetic calorimeter (CEM), central hadron calorimeter (CHA), end wall hadron (WHA), end plug EM (PEM), end plug hadron (PHA), forward EM (FEM) and forward hadron (FHA). All the systems are sampling calorimeters. The central calorimeters consist of plastic scintillators as active volume, while gas proportional chambers are adopted for the plug and forward-backward calorimeters. The properties of the CDF calorimeter systems are summarized in Table 1 and Table 2.

A detailed description of the CDF detector and recent upgrades are found in [1], [2], respectively, and references therein.

Table 1
Properties of the CDF central calorimeters

	CEM	CHA	WHA
η coverage	0.0–1.1	0.0–0.9	0.7–1.3
Number of modules	48	48	48
Number of towers per module	10	8	6
Tower size ($\Delta\eta \times \Delta\phi$)	$\sim 0.1 \times 15°$	$\sim 0.1 \times 15°$	$\sim 0.1 \times 15°$
Number of layers	31	32	15
Active medium	polystyrene scintillator	acrylic scintillator	acrylic scintillator
Scintillator thickness	0.5 cm	1.0 cm	1.0 cm
Absorber	Pb	Fe	Fe
Absorber thickness	0.32 cm	2.5 cm	5.1 cm
Longitudinal samples in tower	1	1	1
Energy resolution @ 50 GeV	2%	11%	14%
Typical position resolution	0.2×0.2 cm^2	10×5 cm^2	10×5 cm^2
Azimuthal boundary gap	3.5 cm	4.1 cm	3.8 cm, 8.9 cm alternating
Depth	$18X_0$	$4.7\lambda_0$	$4.5\lambda_0$
Shower max	strip chamber		

3. Calibrations

The calibration of the CDF calorimeters is described in this section. Especially, the CEM calibration is given as an example to avoid lengthy description of the calibrations for all the calorimeter systems which are basically based on a similar concept, that is, beam tests and gain monitors. For the CEM, however, the calibration insitu has become a main calibration scheme as high statistics of electron data are available, in order to minimise undesirable discontinuity between beam test and real operation. The CEM calibration insitu is also described.

3.1. CEM structure

The CEM is located outside the solenoid and occupies from $R = 1.7$ m to 2.0 m with respect to the beam line. The CHA follows it up to $R = 3.5$ m. The overall dimension is 4.9 m along the beam direction and the calorimeter is separated into two sides at $\eta = 0$. Each side of the calorimeter is further divided to two arches each of which consists of 12 modules with $\Delta\phi = 15°$. Each module forms a single unit called wedge together with the CHA and central muon chamber. Total 10 towers are contained along z (beam direction) in each CEM module. Physical dimension of a tower is about 24 cm in z by 45 cm in ϕ. Light is read out from both ϕ ends and lead to two phototubes separately.

The CEM is a sampling calorimeter with 31 layers of 5 mm thick scintillator and 30 layers of 1/8 inch lead sandwiched. The total depth is $\sim 18X_0$ including the solenoid. There is a gas proportional wire chamber with cathode strips embedded at the approximate EM shower maximum ($\sim 6X_0$) for more precise measurements of EM shower position and shape. One module of the CEM calorimeter is shown in Figure 1.

3.2. CEM calibration

The CEM calibration consists of electron beam test with correlated source runs, periodic source runs since the beam test to monitor gain varia-

Table 2
Properties of the CDF plug and forward calorimeters

	PEM	PHA	FEM	FHA
η coverage	1.1–2.4	1.3–2.4	2.2–4.2	2.3–4.2
Number of modules	2	24	8	8
Number of towers per module	1152	72	360	360
Tower size ($\Delta\eta \times \Delta\phi$)	$0.09 \times 5°$	$0.09 \times 5°$	$0.1 \times 5°$	$0.1 \times 5°$
Number of layers	34	20	30	27
Active medium	Proportional tube chambers with cathode pad readout			
Tube size	0.7×0.7 cm^2	1.4×0.8 cm^2	1.0×0.7 cm^2	1.5×1.0 cm^2
Absorber	Pb	Fe	94% Pb, 6% Sb	Fe
Absorber thickness	0.27 cm	5.1 cm	0.48 cm	5.1 cm
Longitudinal samples in tower	3	1	2	1
Energy resolution @ 50 GeV	4%	20%	4%	20%
Typical position resolution	0.2×0.2 cm^2	2×2 cm^2	0.2×0.2 cm^2	3×3 cm^2
Azimuthal boundary gap	0.9 cm	0.8 cm	0.7 cm (vertical) 3.2 cm (horisontal)	1.3 cm (v) 3.2 cm (h)
Depth	$18X_0$	$6\lambda_0$	$24X_0$	$8\lambda_0$
Shower max	Cathode strip			

tion, and cosmic ray test of each module at the construction stage [3] [4] [5] [6].

The absolute energy scale at the tower center of all the modules was set to 100 pC for 50 GeV/c electrons. Source runs immediately before and after the 50 GeV/c electron beam test were performed to obtain reference calibration values. There are three source calibration systems for the CEM [4], the motor driven ^{137}Cs source scan system which monitors scintillator-WLS-PMT system, the xenon flasher system which monitors WLS-PMT system and the LED flasher system which monitors PMT only. The ^{137}Cs source calibration which was the standard calibration for the energy scale was performed typically once per 3 or 4 weeks. Immediate reproducibility of the measurement of the source response was less than 1%. Beam to ^{137}Cs ratio was found constant within 0.4% by comparing two data sets which were about 5 weeks apart. From these results together with the systematic uncertainty in electron beam momentum, the energy scale from the ^{137}Cs source calibration is known to 1% at most. Calibration by the flasher systems is performed everyday to monitor a short-term gain variation. The xenon flasher system includes PIN diodes to calibrate the fluctuation of the bulb brightness flash-by-flash basis. With this correction, the fractional rms of the response distribution is reduced from 16% to 2%. It is, therefore, easy to achieve an immediate reproducibility of the mean response less than 1%. For the LED flasher system; the fractional rms of the raw distribution is already less than 1%. Three systems monitoring different parts of the light collection system allow us to identify where gain variation comes from. For example, 1.3% increase of the gain is observed when the magnetic field exists which comes from real increase of the scintillator light output.

Several modules were tested to study the energy dependence of the calorimeter performance. The energy resolution is well described by $\sigma(E)/E = 13.5\%/\sqrt{E \sin\theta(\mathrm{GeV})}$.

A response map in a tower relative to the tower center was obtained from the beam scan on all the towers of 5 modules [5]. Cell size in the analysis

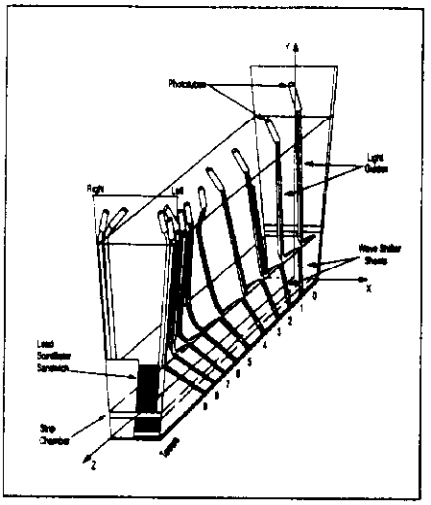

Figure 1. A wedge showing the central EM calorimeter with light collection system.

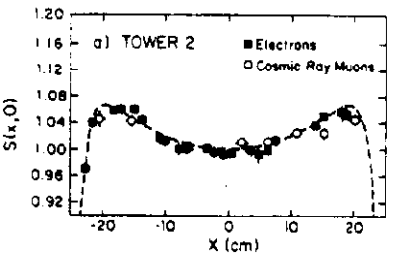

Figure 2. Typical X-dependence of the response at the tower center in z. The X is a local coordinate in a tower along ϕ.

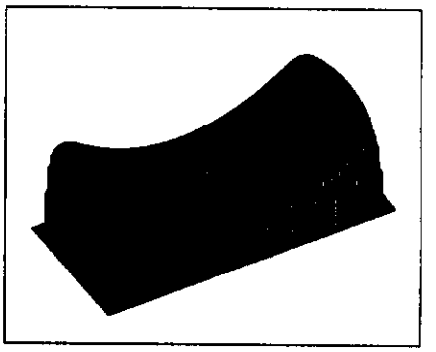

Figure 3. Response map of a CEM tower.

was 1 cm by 1cm and there were 50 × 250 cells in a wedge. With this cell size definition, overall variation of the response, or non-uniformity, was 4%. The response was fitted to a 2 dimensional function for each of 10 tower types. An example of the response as a function of the beam position is shown in Figure 2. The correction function is shown in Figure 3 where the original response function is slightly modified reflecting the in-situ calibration from the 92-93 data. Uncertainty of this correction function which corresponds to the final non-uniformity after the correction was estimated 1–2% including applicability to uncalibrated modules.

The calibration based on the beam test is summarised in Table 3 and Table 4 together with other calorimeters in the central and plug regions.

3.3. CEM recalibration in-situ

The computer controlled ^{137}Cs source scan calibration was initially intended to monitor gain variation of whole the light collection system during data taking runs. It was found, however, that several motor drives broke down in the magnetic field. The source calibration became less preferred to be executed once the detector was rolled in and the solenoid was powered on because of the danger that the sources might be left somewhere in the detector. Instead of performing the source calibration, high statistics of electron data from the 88-89 run and later runs as well made a more realistic in-situ calibration possible looking at energy to momentum ratio (E/P) distribution.

The momentum measured by the central tracking chamber is calibrated using J/ψ, Υ and K_S mass. For the 92-93 analysis, the momentum scale was known to 0.07% from J/ψ mass. The

Table 3
Summary of beam calibrations for the central calorimeters

	CEM	CHA	WHA
Absolute scale	test beam with correlated source calibration		
	e 50 GeV/c	π 50 GeV/c	π 50 GeV/c
• Number of calibrated modules	all towers of all modules		all towers of 2 modules
• Uncertainty	1%	1%	3–5% including applicability to uncalibrated modules
Response map correction (within a tower)	e 50 GeV/c test beam		not done
• Number of calibrated modules	all towers of 5 modules		
• Variation before correction	4%		
• Uncertainty	1–2% including applicability to uncalibrated modules		

average E/P determined from inclusive electron data is scaled to 1 for each tower. Spread of the correction factors including response map correction was 3%. The number of electrons per tower was about 35 which resulted in a statistical uncertainty of 1.7% for the 88-89 run [7]. In the 92-93 analysis, two sets of tower-to-tower calibrations were obtained to minimise the time variation of gains. About 150 electrons per tower for each set resulted in a statistical uncertainty less than 1%. Overall scale factor about +3% was estimated based on Monte Carlo simulation taking into account the photon radiation effect on the E/P distribution. The constant term in the resolution was 2% for the 88-89 run where 1.7% of the statistical uncertainty dominated [8].

Data-determined simple response map was attempted from the 92-93 run, although a complete map for each tower of each module was still not possible. The performance of such a mapping was found comparable to application of the old mapping to newer data. Currently, the original mapping function with a modification based on the in-situ mapping study is used.

3.4. CEM aging

Aging is one of important issues of the calorimeter performance. The aging of the scintillator is estimated by both the source calibration and E/P distribution for electron data. The attenuation length along ϕ of the CEM towers were measured using electron data looking at the energy ratio between left and right phototube output. The decrease of 10% level from 1984-1985 test beam was observed after the 88-89 run. There was no significant change detected in the gain nor the response map within a tower during the 88-89 run. The statistics from this run was relevant only for setting the average tower gain and was not high enough to be sensitive to the time dependence nor the non-uniformity of gains within a tower. For the 92-93 run with higher luminosity, the gain variation along time started seen in the E/P ratio and about 2–3% decrease was observed (Figure 4).

Source calibration data showed about 5% decrease of the response as a detector average from the beginning to the end of the 92-93 run which is consistent with the result from E/P study taking into account for the different time interval looked at in each analysis.

Table 4
Summary of beam calibrations for the plug and forward calorimeters

	PEM	PHA
Absolute scale	test beam with correlated source calibration	
	e 100 GeV/c	π 150 GeV/c
• Number of calibrated modules	one tower of all 2 modules	one tower of one module
• Uncertainty	4%	–
Response map correction (tower-to-tower)	e 100 GeV/c test beam	not done
• Number of calibrated modules	all towers of all modules	
• Variation before correction	4%	
• Uncertainty	1%	

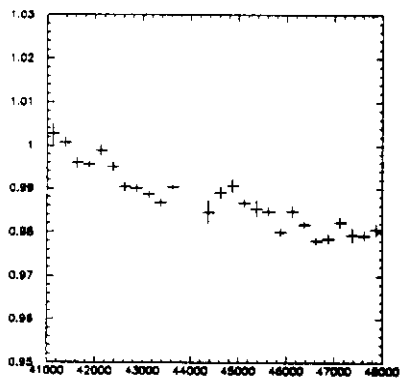

Figure 4. The average E/P as a function of run number for the 92-93 run.

4. Calorimetry in Physics Analysis

4.1. Jet energy correction and resolution

Observed jet energy must be corrected for 1) calorimeter non-linearity for low P_T particles, 2) energy loss in the detector cracks, 3) underlying events and 4) particle-loss out side the clustering window. Underlying event is defined as particle activities originated from soft processes such as fragments from spectator partons in a proton and anti-proton.

The correction function was determined as a function of η using real data and Monte Carlo [2]. A correction relative to the region $0.2 < |\eta| < 0.7$ where no cracks exist was obtained looking at E_T balance in dijet events. Absolute scale correction was estimated by Monte Carlo. Correction for the effect from underlying events was determined from real minimum bias data, and finally particles went out the clustering window are taken into account based on Monte Carlo study. The jet energy correction function is shown in Figure 5. The typical correction factor is 1.3. The energy scale correction was checked using E_T balance in γ+jet events. Uncertainty of the energy scale is about 5% for 20 GeV corrected jets.

The rms resolution of jet energy in the central region was estimated to be $\sigma \sim (0.1E_T + 1)$ GeV looking at E_T balance in dijet events [9]. The absence of a $\sqrt{E}$ behavior for the resolution is due mostly to the presence of long tails in the jet response function associated with energy loss in cracks.

Jet energy scale is well known while the modest resolution and the copious QCD background prevent us from confirming W mass peak in $W \rightarrow 2$ jets events.

4.2. Underlying energy resolution

Underlying energy is usually assumed same as the minimum bias events. The resolution was

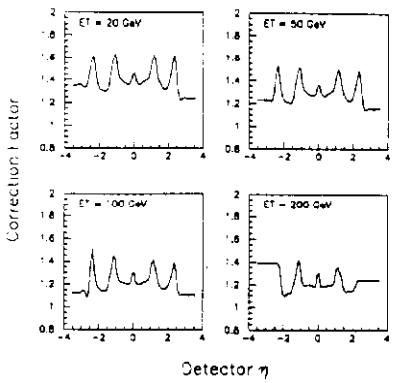

Figure 5. The jet energy correction as a function of detector η for several jet E_T's.

found to be well approximated by $\sigma \sim 0.7\sqrt{\sum E_T}$ from the minimum bias events, where $\sum E_T$ is the total scalar sum of the calorimeter-tower E_T up to $|\eta| < 3.6$ [2].

4.3. Missing E_T correction and resolution

Missing E_T is originally reconstructed from E_T imbalance calculated from the vector sum of calorimeter tower energy within the region of $|\eta| < 3.6$. Missing E_T correction is done by recalculating E_T imbalance from corrected electron E_T and jet E_T with accounting for missing energy due to muons. The resolution is a result of combined effect of electron, jet and underlying energy measurement.

It should be noted that the energy corrections for jet and missing E_T are physics-process and analysis dependent more or less after all.

4.4. Z boson mass

In the remaining subsections, we will discuss more physics-related topics in which the calorimeter performance has much importance.

The mass of Z boson was determined from the 88-89 data using 65 $Z \rightarrow ee$ events [7]. The statistical uncertainty was 0.34 GeV/c^2 while the total systematic uncertainty was 0.43 GeV/c^2 where 0.38 GeV/c^2 came from the calorimetry. The major source of the calorimetry uncertainty was the statistical uncertainty in in-situ calibration. Since precise measurements from LEP have become available, Z events are now used as a check of the electron energy scale. Although the limited statistics ($\sim$ 3000 events for the 92-93 run) makes it less relevant to use them as a calibration tool in the central region where E/P technique can be used, it will be more realistic to calibrate the EM calorimeters using Z events in the plug and forward regions where the momentum measurement is basically not available.

4.5. W boson mass

The W boson mass was measured from $W \rightarrow e\nu$ and $W \rightarrow \mu\nu$ events by fitting a set of transverse mass distributions from Monte Carlo generated over a range of mass and width, to the distribution obtained from data [8] [10]. We consider $W \rightarrow e\nu$ events here.

The transverse mass is calculated from the transverse energy of an electron and a neutrino where the neutrino transverse energy is indirectly measured from visible particle activities as an imbalance of the transverse energy flows. The visible activities are an electron, jet activities recoiling from the boosted W system and underlying events. It is, therefore, important to understand the energy scales for electrons and recoiling jets. The energy resolutions for electrons, recoiling jets and underlying events are also important because they all affect the shape of the transverse mass distribution. In the 92-93 analysis, we did not explicitly separate underlying activities from recoiling activities because increased real Z events allowed us to study the combined effects directly.

We estimated W mass from $\sim$ 1000 events in the 88-89 analysis. The statistical uncertainty was 0.35 GeV/c^2 while the systematic uncertainty was 0.31 GeV/c^2 where the uncertainties from the calorimetry was 0.28 GeV/c^2. For the 92-93 data with increased W events of $\sim$ 6000 and in-situ calibration data, the statistical uncertainty was 0.15 GeV/c^2 and the systematic was about 0.25 GeV/c^2 of which $\sim$ 0.20 GeV/c^2 came from the calorimetry. Further studies are in progress to reduce these systematic uncertainties. Generally,

the energy scale uncertainty was reduced for this run while the uncertainty in understanding of the calorimeter resolution relatively became one of major sources of uncertainties from the calorimetry.

4.6. Top quark mass

The top quark mass is estimated by maximum log likelihood method fitting observed some kinematical distribution with predictions for top of a range of mass, and for background. Several approaches to obtaining the distribution are being studied and most of them try to extract the best estimate of the top quark mass per event and use the resulting reconstructed mass distribution.

A straightforward way of reconstructing top mass is to form an invariant mass from decay particles [2]. For $t\bar{t} \rightarrow e(\mu)+ \geq 4$ jets events where 2 jets originate from light quarks in W decay and other 2 jets from b quarks, we can reconstruct top quark mass if we correctly identify a group of particle objects from each top quark. Since we don't basically know which jet comes from which quark, and there are extra jets radiated off the initial state quarks, we have several possibilities in jet assignments to the quarks. In addition, there are two possible solutions for z component of the neutrino momentum from $M_W = M_{\ell\nu}$. Requiring kinematical constraints, which are $M_{qq} = M_W$ and $M_{\ell\nu b} = M_{qqb} (= M_t)$, within expected errors, the best estimate of the top quark mass is determined. If there exist jets tagged as b by the silicon vertex detector or by identifying a soft lepton in the jet from the semileptonic b decay ($b \rightarrow \ell\nu c$), they are assigned to b quarks which reduces the jet assignment ambiguity. In order to improve mass resolution, invariant mass of the decay products which are assumed from W is fixed to the known W mass.

In this study, it was realised that jet energy correction specific for b jets in $t\bar{t}$ events was necessary which revealed the physics process dependent nature of the jet energy correction. Such a correction was obtained from Monte Carlo. It is also discussed that decay-process dependent correction is necessary for b jets.

It is found jets are correctly assigned in 30% of the events. The resulting rms of the reconstructed top mass distribution for top Monte Carlo is about 20 GeV/c^2 while it is reduced to 10 GeV/c^2 if assignments are all correct. We still need to improve the jet assignment for more precise top quark mass measurement. Part of it will be achieved by looking at more detailed dynamical properties expected for the $t\bar{t}$ production and decay in the standard model.

In this situation, the hadron calorimeter resolution is important. A sufficient jet energy resolution would allow us to identify jets from light quarks which come from W by forming an invariant mass, and reduce other background jets typically existing in hadron collisions.

5. Upgrade Project

5.1. Introduction

The Tevatron collider is to be upgraded from 1997 resulting in a shorter bunch period of 396 ns. According to this upgrade, all the gas calorimeter (plug and forward regions) is replaced with a faster plastic scintillator calorimeter employing optical fibers for readout. The new plug calorimeter which covers from 38° to 3° is a sampling calorimeter with scintillator-absorber sandwich. Scintillator plates are segmented into "tiles" forming a projective tower geometry. The basic properties of the new plug calorimeter are summarised in Table 5.

Since the EM and HAD calorimeter are almost same in their material and structure, details on the development of the new PEM is described. A status of the PHA upgrade is described in [11].

5.2. Structure

One layer of the PEM is physically separated to 24 units each of which covers 15° in ϕ. A 15° unit consists of tiles with readout fibers embedded in, reflectors on both top and bottom surface of tiles and supporting white plastic plates on top and bottom. The number of tiles is 20 for the 1st 15 layers and 18 tiles for the 16th to 23rd layers. Typical size of the tile is 10 cm by 10 cm.

Tiles and reflectors are fixed to the top and bottom plates using two acryl pins per tile. Two pins are positioned at 10 mm inside from the tile corners along a diagonal line. A diagonal line on

Table 5
Mechanical parameters of the CDF upgraded end plug calorimeter

	EM	HAD
Absorber	4.5 mm Pb with 0.5 mm stainless steel on both sides	Fe 5.04 cm
Scintillator	4 mm Polystyrene	6 mm Polystyrene
Total layers	23	22
Total thickness	35.7 cm ($23.2X_0$, $0.96\lambda_0$)	160 cm ($6.8\lambda_0$)
Total units /layer	24 (15°)	12 (30°)
Total tiles /unit	20	36

which pins are aligned is alternated for even and odd layer numbers. Dimension of the pins is 6.5 mm long and 3 mm in diameter.

The top plate has slits at positions on fibers embedded in each tile. A WLS fiber in a tile comes out on the top plate surface through this slit, and near the slit, it is spliced to a clear fiber. Both WLS and clear fiber are 0.83 mm in diameter, and they are fusioned thermally. Another end of a WLS fiber is mirrored by aluminum sputtering and coated with MgF_2 for protection.

There are grooves on the top plates to lead fibers to two optical connectors located at the outer end of the plate. This connector called A-type as a convention houses 10 fibers and connect fibers from tiles to another 10 clear fibers of 3 m long and 0.90 mm in diameter. These 10 fibers are assembled into a flat ribbon cable covered with a black Tedlar film of 50 μm thick. The optical cables from 15° units are routed through the 2.5 cm gap between the central structure and the end plug, to the back of the calorimeter where the fiber cables are connected to 1-m-long and 1-mm-diameter clear fibers at another B-type optical connectors. At these connectors, layer-to-layer arrays of fibers are rearranged into tower-by-tower bundles which are finally connected to phototubes (HAMAMATSU green-extended R4125) via diffusers.

Two stainless steel tubes with 1.3 mm diameter are laid on the grooves on each top plate passing along the center of all tiles. A ^{137}Cs γ-ray source encapsulated at the tip of a finer diameter tubing will be driven into these tubes to monitor gains for each tile.

The new PEM will be also instrumented with a shower maximum detector which consists of two layers of 5 mm wide scintillator strips placed at the 5th EM layer corresponding depth of $6X_0$ [12]. In addition, the 1st layer of the EM will be modified for use as a pre-radiator because its position of about $1.5X_0$ from the collision point is optimum for the discrimination of single photon from π^0. The pre-shower detector will be read out by multi-channel photomultiplier tubes and only difference in the structure is the scintillator thickness of 10 mm to ensure sufficient photostatistics for such phototubes.

5.3. Requirements

Based on the physics demands, the required performance for the new PEM is

- $\left(\frac{\sigma}{E}\right)^2 = \left(\frac{\sigma_A}{\sqrt{E(\mathrm{GeV})}}\right)^2 + \sigma_B^2$

  $\sigma_A \leq 16\%$

  $\sigma_B \leq 1\%$

- Non-linearity $\leq$ 1% for 10–400 GeV.

In order achieve this requirements, we have to control, (1) photostatistics (which affects σ_A), (2) uniformity over tile surface (σ_B, non-linearity), (3) longitudinal uniformity in a tower (σ_B, non-linearity) and (4) cross talk (non-linearity). Based on shower simulations, these requirements are translated to

- > 3 photoelectrons/tile/MIP
  (Sampling fluctuation = 14% out of σ_A = 16%)
- Surface uniformity < 2.5%
- Longitudinal uniformity < 10%
- Total cross-talk < 3%.

Table 6
Light yield decrease after radiation

Sample scintillator	before Light yield(N_{pe})	after 0.5 Mrad Relative decrease in light yield(%)	1.0 Mrad
SCSN81	9.14 ± 0.14	2.2 ± 0.1	8.0 ± 0.2
SCSN38D	10.46 ± 0.14	5.6 ± 0.1	13.6 ± 0.3
BC408	8.95 ± 0.13	8.1 ± 0.2	14.6 ± 0.4

Table 7
Attenuation length before and after radiation

Sample scintillator	before Attenuation length (mm)	after 0.5 Mrad Relative decrease (%)	1.0 Mrad
SCSN81	648 ± 43	32 ± 2	41 ± 3
SCSN38D	402 ± 20	16 ± 1	29 ± 2
BC408	644 ± 12	31 ± 2	32 ± 2

5.4. R&D

The R&D results are summarised here. A more detailed description is found in [13]. Materials for scintillator plate and fiber are determined so as to give the light yield large enough. Tested samples of scintillator plates are Kuraray-SCSN81, 38, 88 and Bicron-BC408. Tested WLS fibers are Kurary-Y11, Y7, B2 and Bicron-BCF91A. Combinations of SCSN38D-Y11 and BC408-Y11 showed high light yield.

The radiation hardness is one of criteria for selecting scintillator. The total radiation dose of 500 Krad for 10 years is expected at $\theta = 3°$ at a luminosity of 10^{31} cm^{-2}sec^{-1}. Required radiation hardness is that the decrease of light yield and attenuation length should be less than 15% and 30%, respectively. Test results of the radiation hardness for several materials are summarized in Table 6 and Table 7. Based on these results, SCSN38D-Y11 was adopted as material for the scintillator and fiber.

The tiles are fixed to the supporting top and bottom plastic plates with pins. In order to minimize the non-uniformity around these pins, several types of pins are tested. Relative light yield at an acrylic pin was about 30%. It was found that the light yield is recovered to about 80% using scintillating pin coated with an acrylic resin. This results in a 98.8% response for 100 GeV electron showers. We performed a heat cycle test for the scintillating pins. The test consists of a temperature change from $-20°$C to $+50°$C per day and this cycle was repeated for 6 days. We found no significant damage on the pins.

The groove path shape, cross-sectional shape and depth were optimised to give especially the best uniformity. Path shape of σ was adopted and the curvature at the tile corners was determined to be 30 mm. A typical response to the β-ray source along the tile center is shown in Figure 6. Increase of the response near the fiber

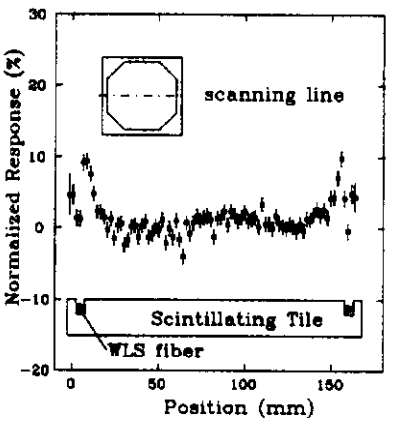

Figure 6. The response variation along a center line on the tile.

corresponds to the increase of the solid angle directly covered by the fiber. When the source is far from the fiber, the solid angle in which the fiber is sensitive to the light is constant which is limited by the critical angle at the tile surface, and it is larger than the one directly covered by the fiber. Getting closer to the fiber, the latter supercedes the former and the sensitive solid angle continues to increase. In order to improve overall uniformity, the groove depth is optimized as shown in Figure 7. We found an empirical relation that

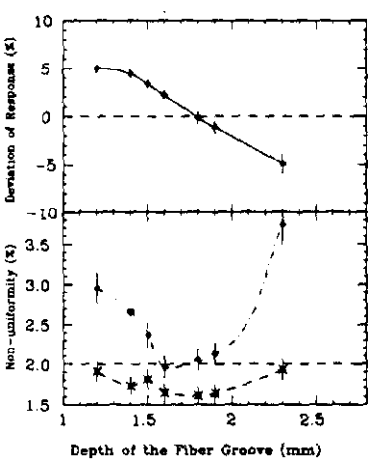

Figure 7. The top plot shows the deviation of the response on the fiber from the one averaged over other region as a function of the groove depth. The bottom plot shows the overall uniformity.

the average response on the groove decreases 1% when the groove depth is deepened by 0.1 mm. The difference between the response averaged on the fiber and the one averaged over the off-fiber region was found dependent on the tile size as shown in Figure 8. The relative response around the fiber to the tile center depends on the tile size due to attenuation of light in the scintillator. An optimum depth is, therefore, dependent on the tile size which can be estimated by the empirical

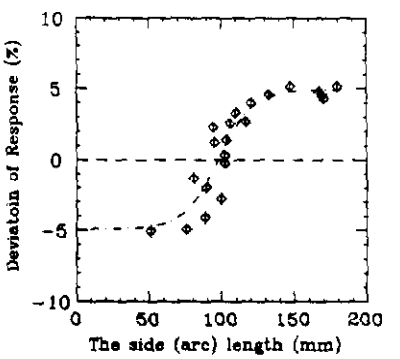

Figure 8. Tile size dependence of the response difference between the average on the fiber and off the fiber.

–1% per 0.1 mm relation.

The splicing is performed by thermal fusion [14]. The light transmission was measured to be 80%.

The mass connector for the fibers was newly developed [15]. There are two types of the connectors shown in Figure 9 and Figure 10. The

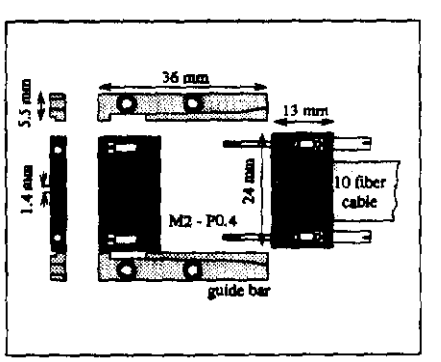

Figure 9. The optical mass connector, type A.

Table 8
Final design of the plug upgrade EM tile/fiber system.

Scintillating tile	SCSN38 (4 mm thick)
WLS fiber	Y11 (multi-clad, 200 ppm, 0.83ϕ) with Al sputtering
Reflector	PET film (E65)
Tile fixture	scintillating pin
Groove path in a tile	r=30 mm at corners
Groove depth	1.5 $\sim$ 2.2 mm depending on the tile size

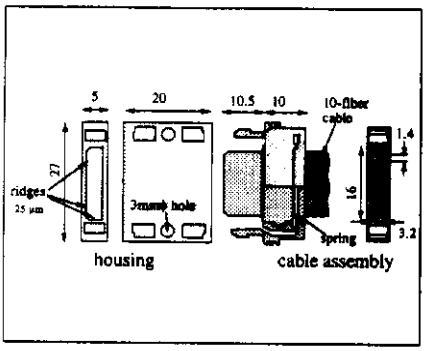

Figure 10. The optical mass connector, type B.

light transmission is 85–90% between fibers with a same diameter. The reproducibility was found 1%. The variation of the light transmission for fibers in a connector was measured $\sim$ 3% for fibers with a same diameter.

The final specifications are summarised in Table 8. We tested the performance of an actual 15° unit. The number of photoelectrons is $\sim$ 7, non-uniformity is 2–2.5% and cross-talk is less than 1%.

5.5. Quality control

The mass production of 15° units was started in October 1993 and completed in February 1994. A total of 1196 units were made. Quality tests which are basically for products sampled at a rate of a few % were done at various production stages.

Thickness of the scintillator mother board was measured at several points and required to satisfy (4 $\pm$ 0.2) mm. Small tile blocks were tested to check if the light yield from the blocks was more than 120 photoelectrons and the variation be less than 2.5%. After tile fabrication, a control fiber was inserted to tiles and tested if the light yield be greater than 12 photoelectrons. Tile-sampling rate was 2% for this test.

Diameter of fiber batches was measured at several points which was required to be (0.83 $\pm$ 0.02) mm. Sampling 4 m fiber at every 50 m and cutting it to 3 m and 1 m, attenuation length for 3 m fiber and light yield for 1 m fiber were tested. Required quality for the attenuation length was 1.5 m $\pm$ 15% for WLS fibers and 10 m $\pm$ 15% for clear fibers. Light yield must be more than 12 photoelectrons and its variation should be less than 5%. After mirroring and splicing, the fiber was exposed by a UV lamp and the light yield was measured by reading current output from phototube. Total 28000 WLS fibers spliced to clear fibers were made and all were tested. The requirement on the light yield variation is 5% for fibers with a same length. Rejecting 1.4% of fibers with more than 10% deviation from the average, the light yield variation was 3.8%.

Assembling fabricated tiles and fibers to 15° unit, light yield, light yield variation in a tower and cross talk were measured using a computer-controlled source scanning system. We measured 10 units from the 12th layer and 1 unit from each of other layers. The light yield from all tiles was larger than 3.5 photoelectrons and the cross talk was less than 2%. The light yield variation of tiles along tower depth direction was 7.9%. All tested pans satisfied our requirements.

All the 15° units will be tested using cosmic ray. A cosmic ray test system was made for this purpose which consists of several crossed-trigger

hodoscopes and drift chambers. It is capable of testing 15 units at a time arranging 15° units in 3 stacks of 5 layers. The units are exposed to cosmic ray for about 1.5 days in which the statistical error of the light yield is less than 1% for most of the tiles. The cosmic ray test of all the units is now underway.

6. Conclusions

The CDF calorimeters were briefly reviewed. Especially the calibration and the performance of the central electromagnetic calorimeter was described in detail. The in-situ calibration based on the energy-to-momentum ratio distribution has become a main calibration technique.

The effect of the calorimeter performance was discussed in Z, W and top quark mass analysis.

The status of the upgrade project for the CDF plug electromagnetic calorimeter was described. The mass production was completed and final test of all the calorimeter subassemblies is underway.

REFERENCES

1. F. Abe *et al.*, Nucl. Inst. and Meth., A271, 387 (1988).
2. F. Abe *et al.*, Phys. Rev., D50, 2966 (1994).
3. L. Balka *et al.*, Nucl. Inst. and Meth., A267, 272 (1988).
4. S.R. Hahn *et al.*, Nucl. Inst. and Meth., A267, 351 (1988).
5. K. Yasuoka *et al.*, Nucl. Inst. and Meth., A267, 315 (1988).
6. R.G. Wagner *et al.*, Nucl. Inst. and Meth., A267, 330 (1988).
7. F. Abe *et al.*, Phys. Rev. Lett., 63, 720 (1989).
8. F. Abe *et al.*, Phys. Rev., D43, 2070 (1991).
9. F. Abe *et al.*, Phys. Rev. Lett., 68, 1104 (1992).
10. R. Keup, CDF Collaboration, Proceedings of the DPF Meeting, Albuquerque, New Mexico (1994).
11. G. Apollinari *et al.*, Fermilab-Conf-94/030-E (1994).
    P. de Barbaro *et al.*, University of Rochester preprint, UR-1360 (1994).
    P. de Barbaro *et al.*, University of Rochester preprint, UR-1371 (1994).
12. P. Melese *et al.*, Rockefeller University preprint, RU94/E-2 (1993).
    G. Apollinari *et al.*, IEEE Trans. Nucl. Sci., 40, 484 (1993).
13. S. Aota *et al.*, Fermilab-Pub-94/240-E (1994), submitted to Nucl. Inst. and Meth. A.
14. K. Hara *et al.*, Nucl. Inst. and Meth., A348, 139 (1994).
15. S. Aota *et al.*, "Development of Fiber-to-Fiber Connectors for Scintillating Tile/Fiber Calorimeters", submitted to Nucl. Inst. and Meth. A.